A Flexible Coupled Ocean–Atmosphere General Circulation Model①

Yu Yongqiang (俞永强)②, Yu Rucong (宇如聪), Zhang Xuehong (张学洪) and Liu Hailong (刘海龙)

LASG, Institute of Atmospheric Physics, Chinese Academy of Sciences, Beijing 100029

(Received February 28, 2001; revised August 15, 2001)

ABSTRACT

Based on the National Center for Atmospheric Research (NCAR) Climate System Model version 1 (CSM–1), a Flexible coupled General Circulation Model version 0 (FGCM–0) is developed in this study through replacing CSM–1's oceanic component model with IAP L30T63 global oceanic general circulation model and some necessary modifications of the other component models. After the coupled model FGCM–0 is spun up for dozens of years, it has been run for 60 years without flux correction. The model does not only show the reasonable long–term mean climatology, but also reproduce a lot of features of the interannual variability of climate, e.g. the ENSO–like events in the tropical Pacific Ocean and the dipole mode pattern in the tropical Indian Ocean. Comparing FGCM–0 with the NCAR CSM–1, some common features are found, e.g. the overestimation of sea ice in the North Pacific and the simulated double ITCZ etc. The further analyses suggest that they may be attributed to errors in the atmospheric model.

Key words: Coupled model, ENSO, Climate drift

1. Introduction

Global coupled ocean–atmosphere general circulation models (CGCMs) are now becoming important tools to study climate variability and climate change induced by external forcing. For example, the National Center for Atmospheric Research (NCAR) Climate System Model version 1 (CSM–1) (Boville and Gent, 1998, hereafter referred to as BG98 in this study) has been widely used in climate studies, and it reproduces a lot of important characteristics of contemporary climate (Meehl and Arblaster, 1998). The model contains an atmospheric model and an oceanic model, a land process model, and a thermodynamic and dynamic sea ice model. These component models communicate through a flux coupler, which controls the time coordination of the integration and calculates most of the fluxes at the interface of the model components. Although no flux correction in momentum, heat and fresh water fluxes is applied, the model does not show any significant climate drift in a 300–year integration.

A lot of coupled GCMs including CSM now show pretty good ability to simulate the fundamental features of climate system, but there are some uncertainties induced by cloud, turbulence flux etc. in models' simulations. An effective procedure to understand these uncertainties is intercomparison between model and observation or model and model. In fact,

①This study is jointly supported by Chinese Academy of Sciences under Grant "Hundred Talents" for "Validation of Coupled Climate Model", Chinese Academy of Sciences (CAS) "Innovation Programme" under Grant ZKCX2–SW–210 and NSFC under Grant No. 49823002.

②E–mail: yyq@lasg.iap.ac.cn

the latter has been commonly adopted, for example both the Atmospheric Model Inter–comparison Project (AMIP) (Gates, 1992) and the Coupled Model Inter–comparison Project (CMIP) (Meehl et al., 2000), from which scientists have learnt a lot of important and interesting points, are international corporation projects containing dozens of climate models. Therefore, it is a beneficial idea to substitute the oceanic or atmospheric component model of CSM with the other model then compare its simulation with those from the origin CSM version, because it will help us partly understand the reason of model's problems such as climate drift and the double ITCZ etc. In this study, the oceanic component model of CSM–1 is replaced with another OGCM successfully, which is developed in the Laboratory of Numerical Modeling for Atmospheric Sciences and Geophysical Fluid Dynamics (LASG), Institute of Atmospheric Physics (IAP) (Jin et al., 1999). There have been three generations of global coupled models developed in the IAP in the past decade (Zhang et al., 1992; Chen et al., 1997; Wu et al., 1997), but the above current coupled model is very different from these coupled models in the configuration of models, because it is a Flexible coupled General Circulation Model (hereafter referred to as FGCM), in which it is easy to replace any component model with another one.

The purpose of this study is to describe the major characteristics of a 60–year integration from FGCM–0 especially the mean climatology and the interannual variability, and compare them with those from NCAR CSM–1. It is organized as follows. Section 2 describes model components and flux coupler, as well as the coupled model spin–up procedure. The multi–year mean climate simulated by FGCM–0 is shown in section 3. Section 4 describes the ability of FGCM–0 to reproduce the interannual variability in the tropical Pacific and Indian oceans. Section 5 is summary and discussion.

2. Model description

The oceanic component model used in the coupled model is the third–generation global OGCM developed at IAP by Jin et al. (1999). Its horizontal grid system is just the same as that of a T63 spectral atmospheric general circulation model (AGCM) with the grid size of about $1.875^\circ \times 1.875^\circ$. There are thirty layers in the vertical, of which twelve equal depth layers are placed in the upper 300 m for depicting the equatorial thermocline better. In short, the model is often called " L30T63" . Some fairly mature parameterizations are adapted to the model, including the penetration of solar radiation (Rosati and Miyakoda, 1988), the " PP" scheme for the upper ocean vertical mixing (Pacanowski and Philander, 1981), and the isopycnal mixing scheme proposed by Gent and MacWilliams (1990). A thermodynamic sea–ice model based on Parkinson and Washington (1979) is also incorporated into the ocean model. The model was first integrated for 1160 years with the wind stress forcing of Hellerman and Rosenstein (1983) and the thermal forcing required in a Haney–type formula for heat–flux (Haney, 1971), taken from the COADS (Comprehensive Ocean–Atmosphere Data Set) (da Silva et al., 1994). The model's surface salinity was simply relaxed to the climatological annual cycle of Levitus and Boyer (1994). By the end of the integration, the model reaches a quasi–equilibrium state, of which both the wind–driven circulation and the thermohaline circulation are reasonably simulated (Jin et al., 1999). This may be seen as the L30T63's basic run that provides initial conditions for the coupled model spin up run. Forced by the month–by–moth wind stress over the tropical Pacific Ocean from the ECMWF Reanalysis (ERA) data for the time period from 1980 to 1989, the OGCM reproduces the reasonable interannual variability in the tropical Pacific Ocean (Yu et al., 2001).

The coupled ocean–atmosphere general circulation model (CGCM) used in this study is the primary version of a Flexible General Circulation Model for climate system (referred to as FGCM–0). The FGCM–0 is formulated based on the NCAR CSM–1 (BG98) by replacing the CSM–1's ocean component, NCOM (the NCAR CSM Ocean Model), with the L30T63 in virtue of the CSM's flux coupler. The functions of the flux coupler are: 1) controlling the time coordination of all the component models of the climate system model; 2) calculating most of interfacial fluxes; 3) communicating with component models for exchanging fluxes and some control parameters (Fig. 1). The flux coupler is also responsible for interpolating and averaging between the different grid systems of component models while conserving local and integral properties. As pointed out already in BG98, the coupling strategy (based on the flux coupler) allows component models to be exchanged relatively easily. In fact, it provides an efficient way to formulate a new climate system model and to test the sensitivity of the model to any of its component models. The FGCM–0 represents just the first step towards a fully developed FGCM, of which the oceanic component is the OGCM, L30T63 (without using its thermodynamic sea–ice component), and the others are almost the same as those in the CSM–1. The atmosphere and land surface components are the CCM3 (the Community Climate Model, Version Three, see Kiehl et al., 1998) and the LSM1 (Bonan, 1998), respectively. Since the geography of the FGCM–0 is identical with that of the L30T63, the land–sea marks and surface types of the CCM3 have been modified to match the OGCM. Also, the horizontal grid system of the sea ice model of Weatherly et al. (1998) has been modified to be same as that in the original L30T63. The atmospheric, land and sea ice model communicates with the flux coupler every model hour, and the oceanic model every model day.

To diminish the initial shock in the coupling process, a spin–up procedure is adopted before running the FGCM–0.

Firstly, the AGCM, CCM3, and the land surface model, LSM1, are integrated for five years by using the observed climatological sea surface temperatures (SST), sea–ice distributions based on Shea et al. (1990) and the same land–sea mask as the ocean component model L30T63. This five–year integration is referred to as "Run 1" in this study. Daily data from the last four years of Run 1 are archived for state variables and for radiation flux at the lowest model level.

Secondly, the OGCM, L30T63, in association with the thermodynamic sea ice model of

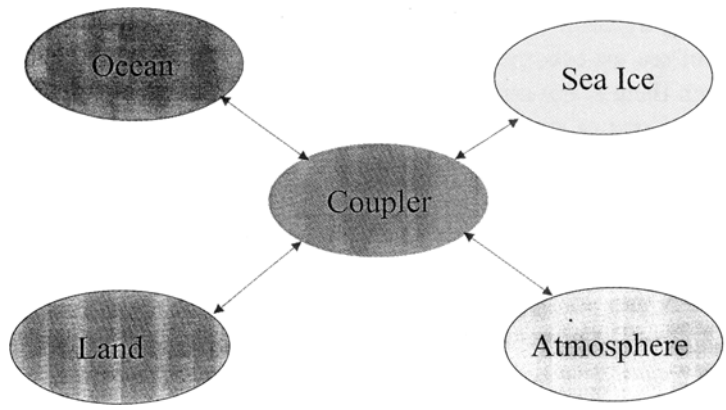

Fig. 1. The FGCM–0 component models configurations.

Weatherly et al. (1998) is integrated for seventy years, started from the year 1160 of the ocean model's basic run mentioned above. In the course of the integration, the surface wind stress and thermal forcing were taken from the daily state variables and radiation flux for the last four years of the aforementioned CCM3 run. For the surface salinity, the restoring condition is still used, without considering the fresh water flux calculated based on the AGCM and OGCM themselves. This seventy-year integration of the ocean model will be referred to as "Run 2" or "Spinup Run".

Following the spinup step, the fully coupled model, FGCM-0, was integrated for sixty years. The initial conditions for the atmosphere, land surface, ocean and sea ice models are taken from the end of the Run 1 and Run 2, respectively. As in the CSM-1, the atmosphere and ocean-sea ice models in the FGCM-0 were directly coupled by exchanging the heat and momentum fluxes themselves, rather than the flux-anomalies as in the previous IAP/LASG CGCMs (Yu et al., 2000). Different from the CSM-1, the fresh water exchange was not included; instead, the relaxation condition of salinity was still used in the FGCM-0. Also in order to diminish the initial shock, the dynamic process of sea ice was not included until the end of the first seven years of the coupled integration.

Although there is moderate difference between simulations from the ocean-only model in the basic run and ocean model spinup run in Run 1, both the two simulations describe very similar large scale pattern of ocean circulation compared with coupled simulation (Zhang and Yu, personal communication).

3. Long-term mean climatology

The FGCM-0 has been integrated for 60 years. The monthly global mean sea surface temperatures (SSTs) shown in Fig. 2a does not exhibit a significant cooling or warming trend, e.g. the difference of global mean SSTs from the first and second 30-year runs is only $-0.1^{\circ}C$ that is much less than its interannual and interdecadal variability. Figure 2a also shows the stronger oscillation at the interannual and interdecadal time scale during the first 30 years than that during the last 30 years, which may be associated with the variation of sea ice as shown in the following analyses. Figures 2b and 2c show the area of simulated sea ice in the Northern and Southern Hemispheres together with the observational annual ranges of sea ice indicated by straight lines from Gloersen et al. (1992), respectively. In the Southern Hemisphere, an abrupt decrease in the area of sea ice around the 8th model year should be attributed to introducing dynamic process of sea ice in the model at that time as described in section 3. The area of sea ice becomes stable in the Southern Hemisphere 10 model years later. However, although there is not any obvious change around the 8th model year in the Northern Hemisphere, the area of sea ice has been increasing in the first 40 model years that is responsible for the cooling trend in global mean SST. In fact, there is not any cooling or warming trend in the tropical central Pacific and Indian oceans (see Figs. 8, 10a and 10b). When the total area of sea ice becomes stable after the 40th model year, it is overestimated about 30% in the Northern Hemisphere compared to the observation annual ranges. The excess is somewhat larger in winter than in summer. In contrast, the simulated sea ice in the Southern Hemisphere is very close to the observational one. The overestimation of sea ice in the Northern Hemisphere is very similar to that given by CSM-1 (see Fig. 11 in BG98). Because the only difference between CSM-1 and FGCM-0 is OGCM, the atmospheric and land model should be responsible for this overestimation.

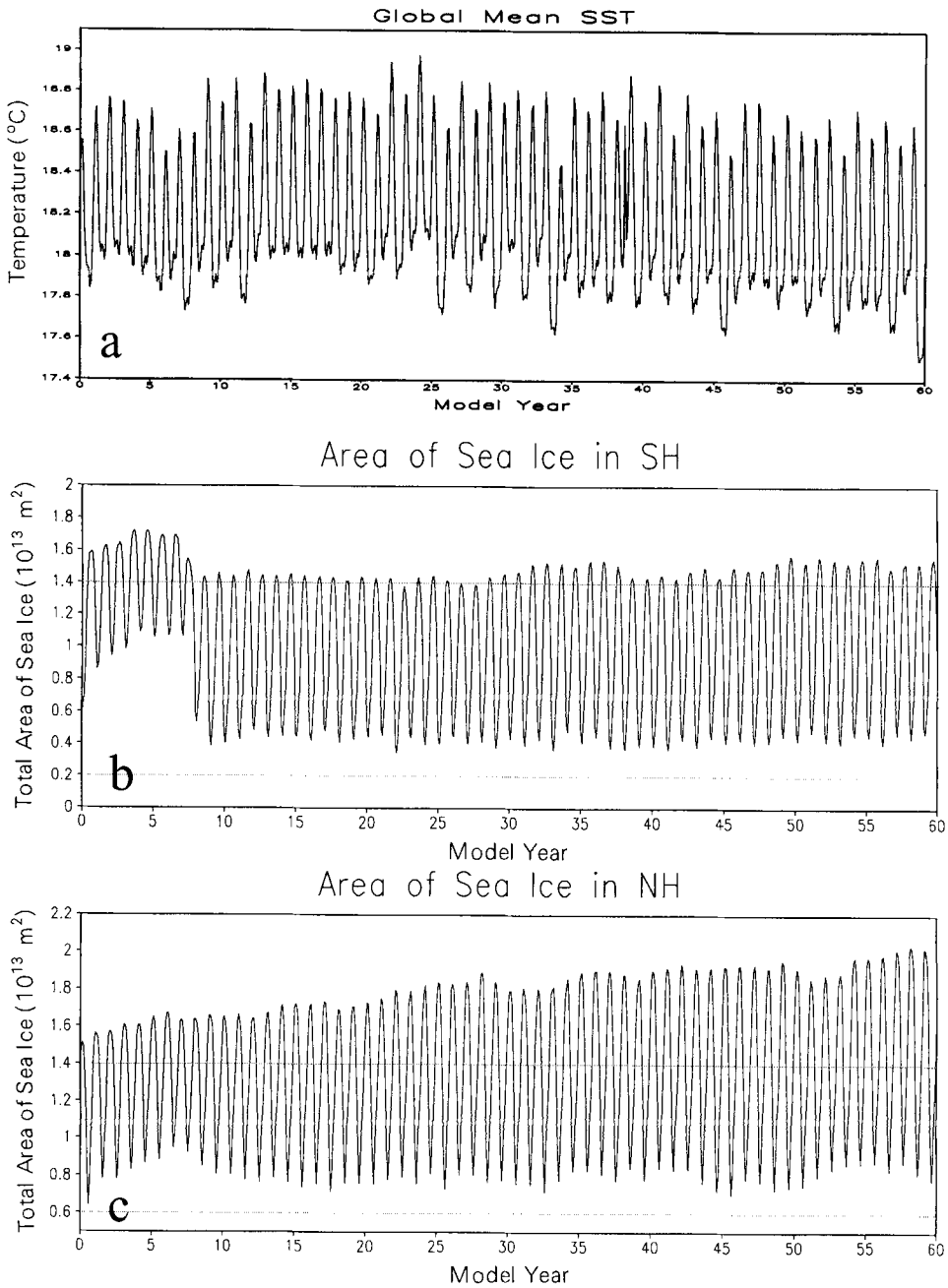

Fig. 2. The time series of (a) monthly global mean sea surface temperature (°C), the total area of sea ice (10^{13} m^2) in (b) the Southern Hemisphere and (c) the Northern Hemisphere, the straight lines indicate the observational maximum and minimum area of sea ice.

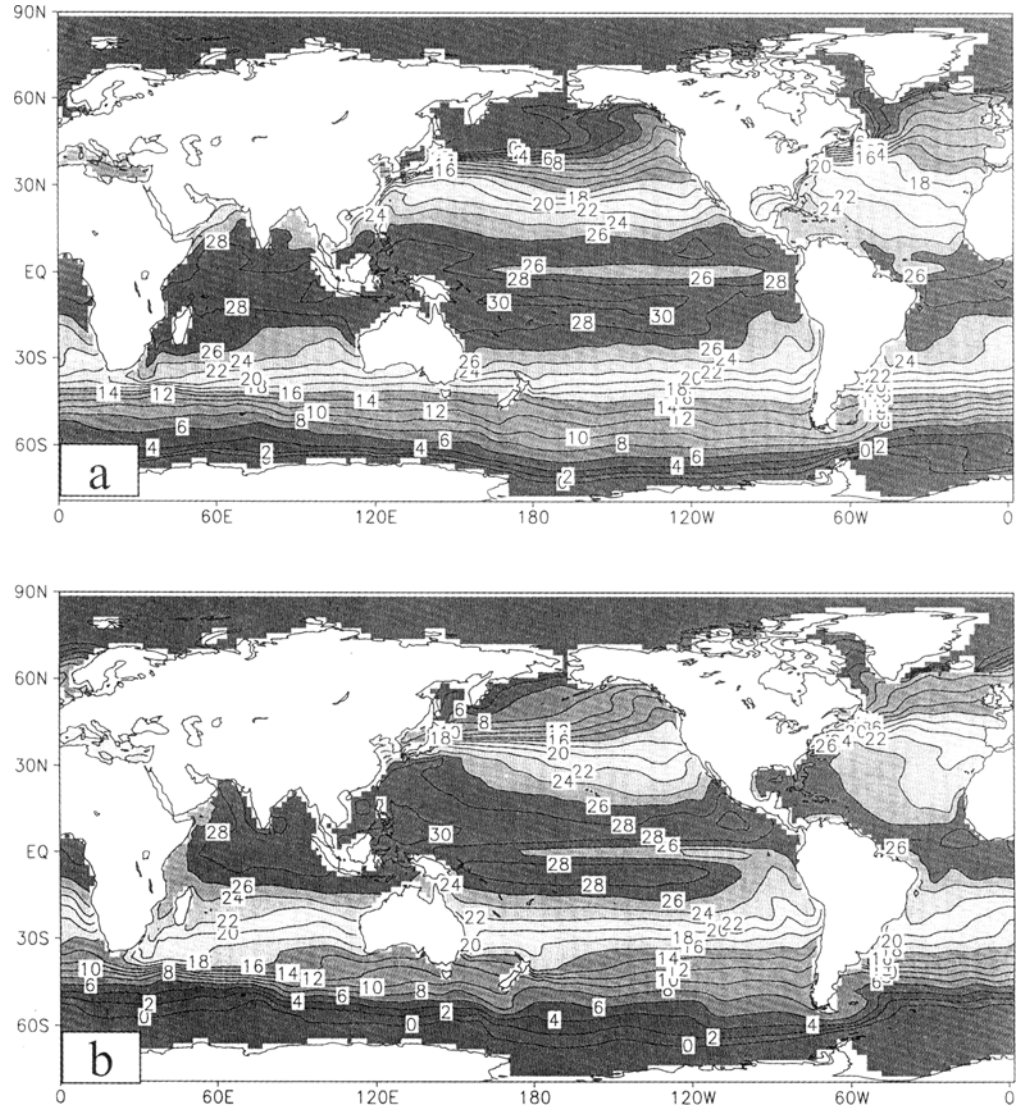

Fig. 3. Simulated sea surface temperatures (°C) averaged from 11th to 60th model year for (a) March and (b) September.

The simulated climatological SST for March and September are shown in Figs. 3a and 3b. Although the warmer water is simulated in the off–equatorial oceans in the Southern Hemisphere and the colder water in the North Pacific than those from observation, the large pattern of SST is acceptable compared with the other direct coupling models (Mechoso et al, 1995; BG98). Figs. 4a and 4b exhibit the difference between simulated SST from the coupled model and spin up run for March and September. It is very interesting that the coupling among four component models results in warming in most area of the Southern Hemisphere and cooling in most area of the Northern Hemisphere, respectively. The combined impacts of the warming and the cooling is the decrease in the global mean SST about 0.1°C only during 60 years run as described above. The significant warming in the Antarctic Circumpolar

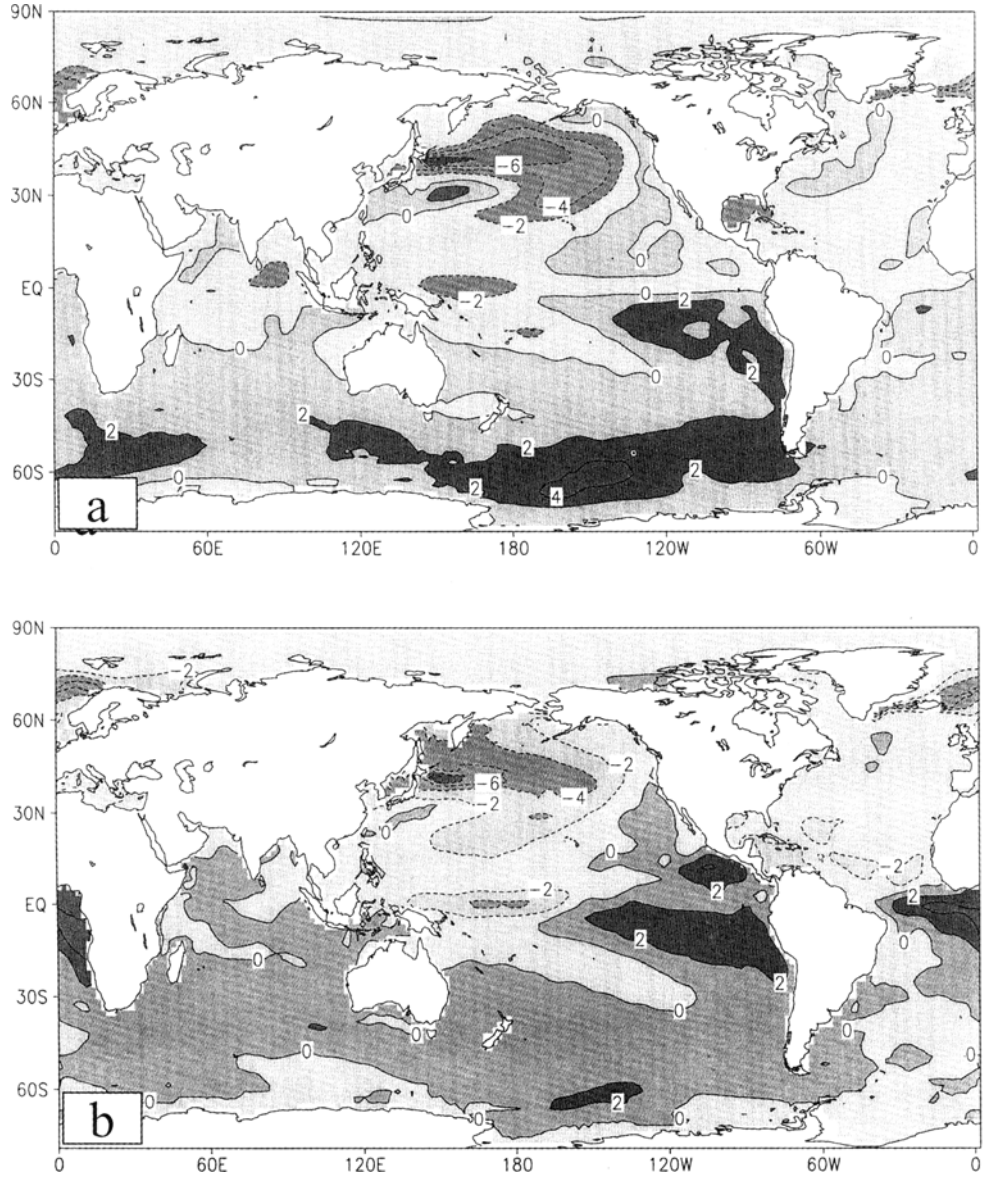

Fig. 4. The SST difference (°C) between coupled simulation and spinup run for (a) March and (b) September.

Current (ACC) region is associated with the variation of sea ice. In the spin up run, because the dynamic process of sea ice is not introduced in the model, melting or freezing of sea ice is dominated by the local heat flux only. Once the dynamic process of sea ice is considered, it becomes possible that sea ice drifts to the region with warm water and then melts rapidly. Because ACC is much stronger than any currents in the Arctic Ocean, the velocities of sea ice in the Southern oceans are much larger than those in the Arctic Ocean. Thus, it is easier for sea ice to drift to the warm region and be melted in the Southern Hemisphere in the coupled model, which results in much more solar flux into the ocean and in turn significant warming in this

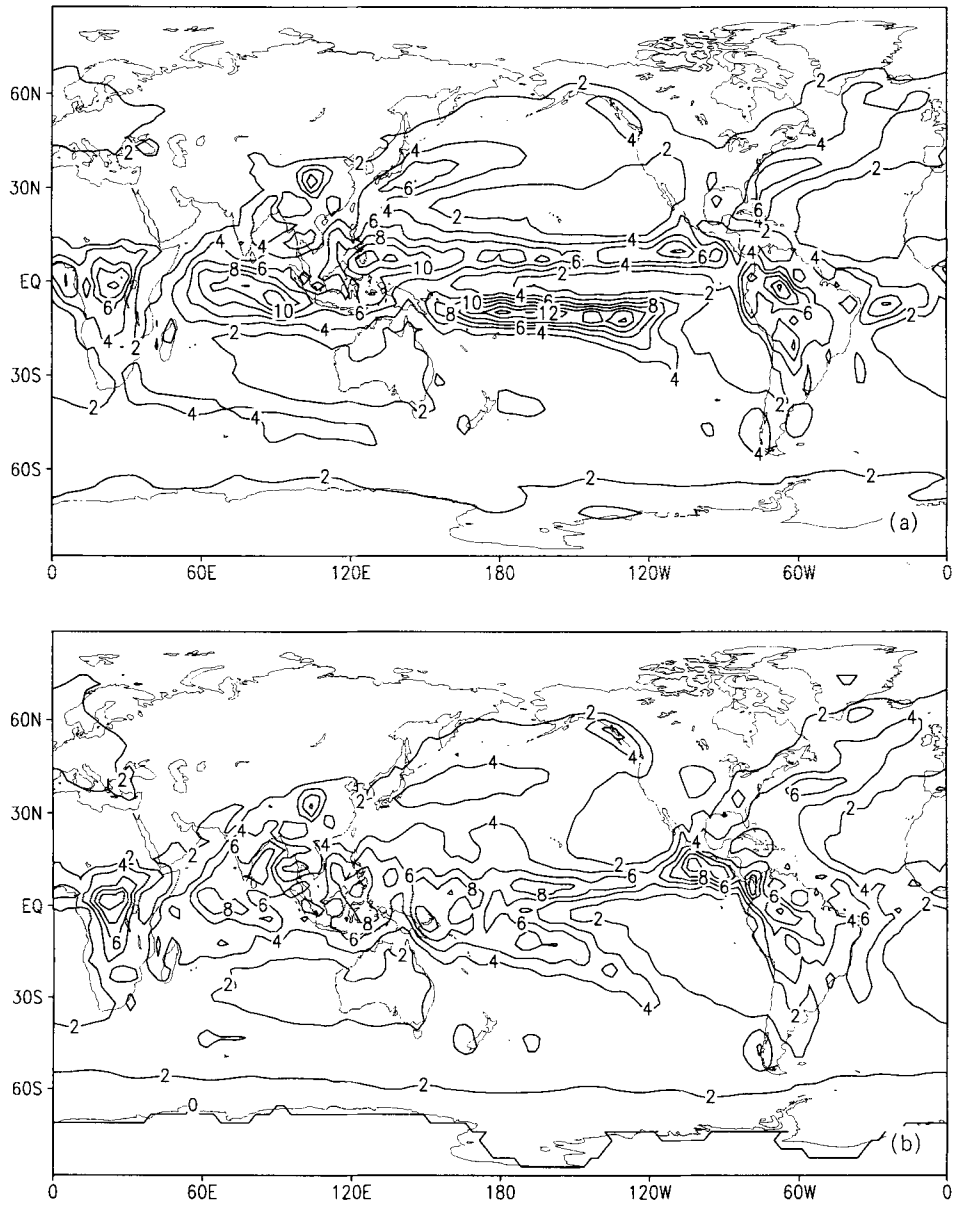

Fig. 5. Simulated annual mean precipitations (mm / day) averaged from 11th to 60th model year for (a) the coupled model and (b) the uncoupled CCM3.

region compared to spin up run. The strong cooling center in the North Pacific is related to the southward extension of sea ice, which shows about 10° southward displacement during wintertime (not shown here) compared to the observational one. Although the simulated extension of sea ice in the North Pacific from CSM−1 is somewhat better than that in the coupled model, CSM−1 overestimates the area of sea ice too much in the winter in the Northern Hemisphere (see Fig. 13 in BG98). This is because that the air temperature simulated by the

atmosphere–only model CCM3 near the northwest Pacific coast shows a cold bias about 5–10°C as described by Bonan (1998). In a coupled model, the air–ice–sea interaction will amplify the initial error from the uncoupled AGCM due to the so–called ice–albedo–temperature positive feedback mechanism and result eventually in much increase in the extension of sea ice. Because the simulated cold tongue extends to far west, and the warm pool is pushed southwestward (Fig. 3), a cold bias in the central and western Pacific and a warm bias can be found from Fig. 4 in the eastern Pacific and off the equator, respectively. These errors in the climatological state from the coupled model still induce a lot of changes in the oceanic and atmospheric circulations.

Figures 5a and 5b show the annual mean precipitation from the coupled model and uncoupled AGCM, respectively. Forced with climatological SST from Shea et al. (1990), the CCM3 simulated the major precipitation belts such as the inter–tropical convergence zone (ITCZ), the South Pacific convergence zone (SPCZ) and Asian monsoon system etc. (Fig. 5b). There is not evident difference between the large–scale patterns of precipitation from the atmosphere–only model and the coupled model at middle–high latitudes. But the tropical precipitations are significantly different between these two simulations. Unlike the uncoupled CCM3, the coupled model fails to simulate the SPCZ but shows highly symmetric ITCZs about the equator, e.g. the so–called "double ITCZ" (Mechoso et al., 1995), while both the observations (not shown here) and the atmosphere–only model CCM3 show only ITCZ in the Northern Hemisphere permanently. The simulated northern ITCZ in the coupled model is much less than that in the atmosphere–only model in the central and western Pacific, where there is cold bias in SST from the coupled model. In contrast, the simulated southern ITCZ is much stronger than the atmosphere–only simulation in the southeastern Pacific, where there is a warm bias in SST from the coupled model. These are very common features for the directly coupled ocean–atmosphere models, as mentioned by Mechoso et al. (1995) and BG98. The simulated double ITCZ results directly from errors in SST from the couple model, but the ultimate causes can be traced back to models' physical parameterizations. Philander et al. (1996) argued that the double ITCZ might be caused by too much net downward solar radiation off the western coasts of South America, while Kiehl et al. (1998) argued that it should be associated with overestimation of net downward solar radiation at the western equatorial Pacific Ocean. Moreover, the former suggested that an underestimation of low–level stratum clouds in AGCM should be responsible for the double ITCZ, while the latter suggested that an underestimation of model cloud shortwave absorption in the western tropical Pacific was the fundamental reason. In order to discuss the possible causes for the double ITCZ in the coupled model, the comparison of solar radiation among atmosphere–only model, the coupled model and observation is conducted as follows.

The simulated net downward solar flux derived from spin up run and the coupled model are shown in Figs. 6a and 6b, respectively. The observed solar radiation from da Silva et al. (1994) is shown in Fig. 6c, which is used to force the individual OGCM in this study. The large–scale spatial pattern of the simulated solar radiation in the spin up run is very similar to the observational one. However, the former, outputted from the atmosphere–only model CCM3, overestimates the net downward short wave radiation at the sea surface in most regions of the tropical Pacific Ocean, especially in the warm pool and the southeastern Pacific Ocean about 20 W/m^{-2}. Because the net downward heat flux is very small (15–30 W/m^{-2}) in these two regions, it is easy for the overestimation of solar radiation to alter the spatial

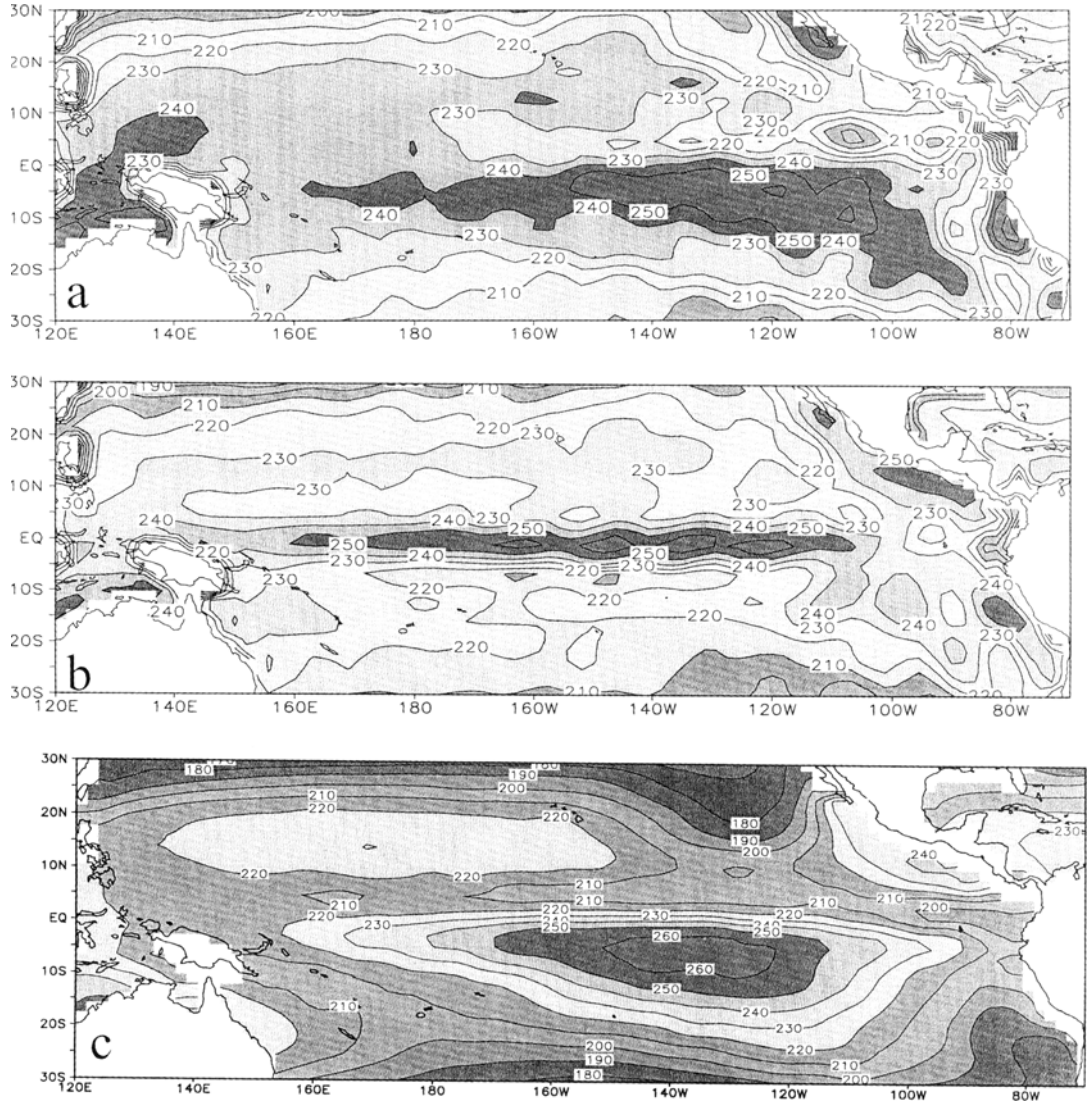

Fig. 6. Simulated net downward annual mean solar radiation (W m^{-2}) for (a) uncoupled CCM3, (b) the coupled model FGCM−0 averaged from 11th to 60th model year, and (c) observation.

pattern of the simulated warm pool and cold tongue through the air–sea interaction as discussed in the following analysis.

In the tropical oceans, heat fluxes contributing to heat budget are solar flux and latent flux, which dominate the tendency of temperature at the sea surface. Thus the overestimation of solar radiation should be balanced by the latent heat flux. In the coupled model, the latent flux is calculated according to the following formula:

$$F_{\text{lat}} = \rho C_{\text{d}} L |\vec{V}| (q_{\text{a}} - q_{\text{s}}) \ , \tag{1}$$

where F_{lat} is the latent flux that depends on the air density ρ, drag coefficient C_{d}, evaporation potential heat L, scalar wind velocity $|\vec{V}|$, air humidity q_{a} and saturation humidity at the

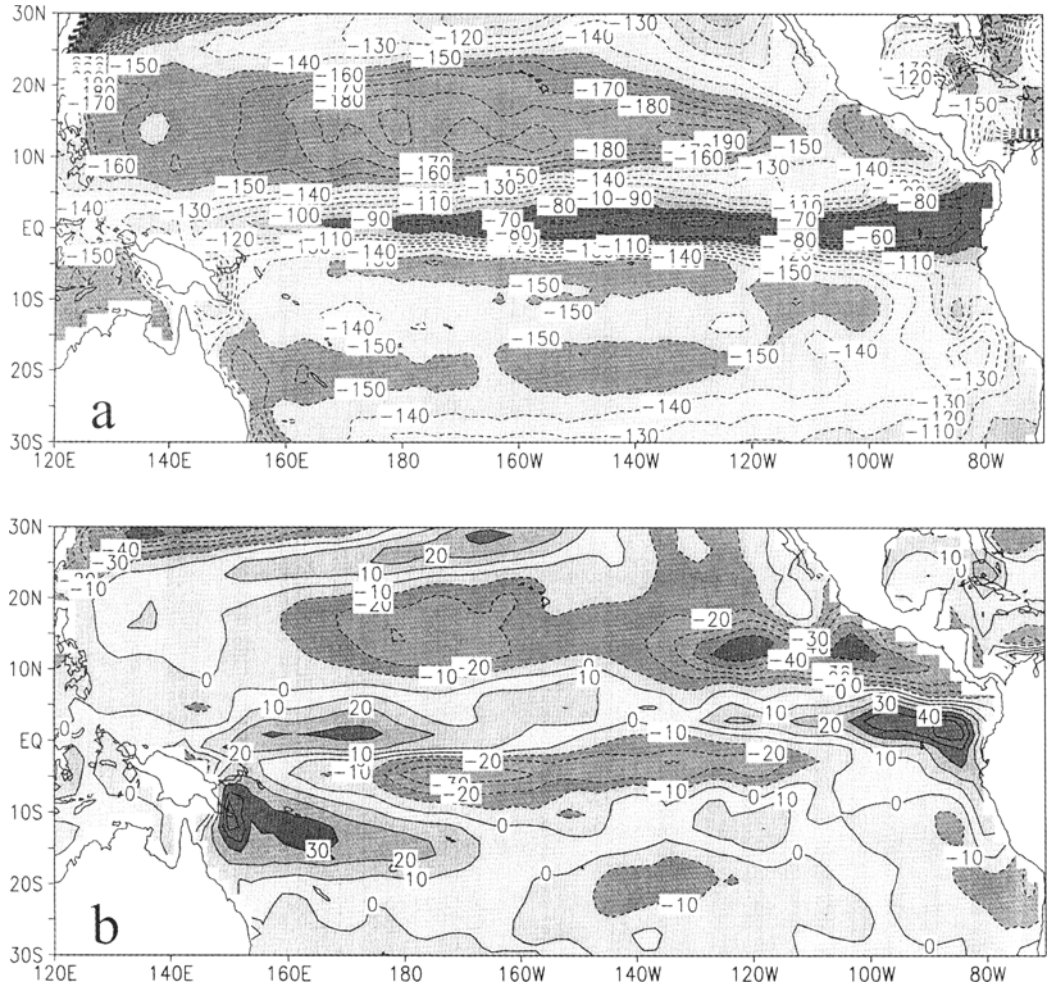

Fig. 7. (a) Simulated annual mean latent flux (W m^{-2}) for the uncoupled CCM3 and (b) the difference of latent flux (W m^{-2}) between the coupled model FGCM−0 averaged from 11th to 60th model year and the uncoupled CCM3.

sea surface q_s that only depends on SST. In short, we consider both ρ and C_d as constants. In the spin up run, the ocean model is forced by the atmosphere−only mode CCM3 daily output variables such as surface air temperature, wind, specific humidity etc. In order to balance the overestimation of solar radiation in the western tropical Pacific and southeastern Pacific Ocean, the latent flux have to increase compared with the individual OGCM forced with the observational climatology. In the "Spin up" run or "Run 2" as described in section 3, both the scalar wind velocity and the air humidity are the external forcing variables derived from the atmosphere−only model CCM3 and are independent of the simulated SST. The saturation humidity at the sea surface q_s is the only variable that contributes to the increase in the latent flux in terms of Formula (1), which implies than the simulated SST is warmer than that by the ocean−only model. In fact, the simulated SST is a little warmer in the warm pool region in the spin up run than the ocean−only model forced with the observed climatology (not shown) in the "Basic Run".

In the coupled model, the response of the model to overestimation of solar radiation becomes more complex due to the air–sea interaction, because it is cancelled by the increase in either cloud, which can reflect more short wave radiation to outer space, or latent flux. In the warm pool region, the warmer SST results in stronger zonal wind because the zonal gradient of SST increases, then the stronger zonal wind in turn enhances upwelling in the equatorial eastern Pacific that decreases SST off the eastern coast and increases the zonal gradient of SST. This is a positive feedback, finally it results in very strong zonal wind (not shown) and 2–3°C cooling in the western Pacific as shown in Fig. 4. As indicated above, the simulated SST is warmer in the spin up run than the individual OGCM run in the warm pool region, thus the zonal gradient of SST is stronger than that from the individual OGCM run. However, in the southeastern Pacific, where the subtropical high is located, the overestimation of solar radiation results in the warmer SST that weakens the subtropical high and wind and increases cloud and precipitation, which in turn augments SST again. Finally, about 2°C warming in SST associated with the double ITCZ occurs in the southeastern Pacific Ocean due to the air–sea interaction (see Figs. 4 and 5). The simulated latent flux shown in Fig. 7 confirms our hypotheses above, there is significant increase of latent flux in the coupled model in comparison with the individual OGCM in the tropical central and western Pacific, which cancels the overestimation of the solar radiation; in the southeastern Pacific, the difference of the latent fluxes between the coupled model and the individual OGCM is very small, because the overestimation of the solar radiation is cancelled by increase in cloud.

4. Simulation of interannual variabilities over the tropical Pacific and the Indian Ocean

Forced with the observed wind stress, the oceanic component model has shown good ability in reproducing El Niño and La Niña events during the 1980s (Yu et al., 2000). When the oceanic model is coupled to the atmospheric, land and sea ice models through the flux coupler, the interannual variation of the averaged SST over the Niño 3.4 region (170°–120°W, 5°S–5°N) is produced automatically without any external forcing except for solar radiation, implying that the coupled model can simulate the "ENSO–like" phenomena (Fig. 8). The coupled model produces very similar amplitude of Niño index to the observational one, but shows a quasi–biennial oscillation only instead of a considerable wide period from 2 to 7 years as in the real world.

As discussed above, the FGCM shows some ENSO–like characteristics in the interannual variation of SST in the eastern equatorial Pacific. Here we examine the time–space features associated with oceanic and atmospheric circulations in the model. Figure 9 shows lag correlations between the Niño 3.4 index and SST, zonal wind stress, vertically averaged temperatures (VAT) in the upper 300 m as an indicator of heat content in the equatorial and off–equatorial oceans. In Fig. 9a, the SST anomaly propagates westward very fast off the eastern coast, but it shows some features like standing oscillation in the central equatorial Pacific. The zonal wind stress shows the similar feature of propagation (Fig. 9b), while the westerly wind anomaly leads the warm SST anomaly about 2 to 5 months off the eastern coast, but only 1–2 month in the central equatorial Pacific. It is interesting that VAT shows an eastward propagation with a phase speed about 0.6 m/s. At the equator, the positive VAT anomaly occurs near the western boundary about 9 months prior to the mature phase of El Niño events (lag = –9 months), then propagates eastward (Fig. 9c), which induces an initial warm SST anomaly off the eastern coast (Fig. 9b); at lag = 3 months, a negative anomaly

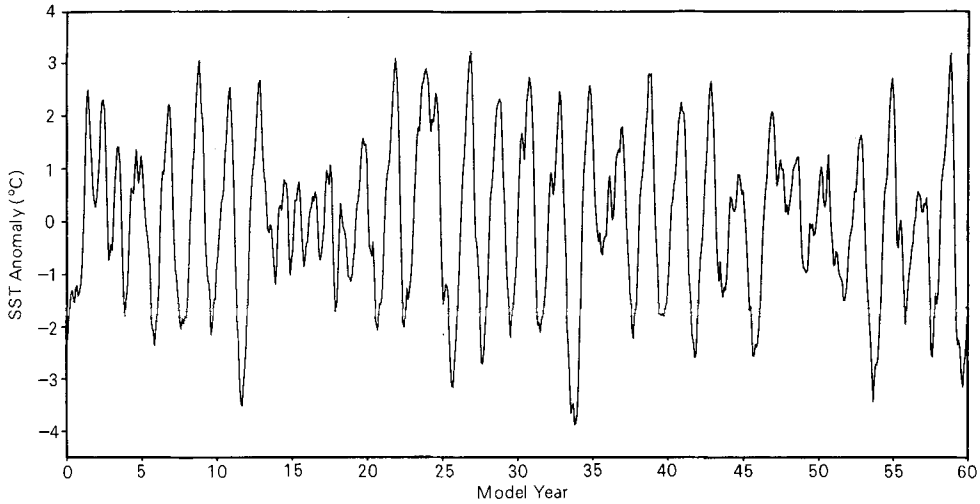

Fig. 8. Simulated sea surface temperature anomalies (°C) averaged over Niño 3.4 region (170°–120°W, 5°S–5°N).

occurs at the western boundary then moves eastward, which ends the current El Niño and intrigue the next La Niña event. Out of the equator (5°–8°N), the VAT anomaly propagates westward with very slow speed in the eastern Pacific and very fast speed in the central and western Pacific (Fig. 9d). The negative VAT anomaly off the equator occurs at the eastern boundary and shifts westward about one year prior to the mature phase of El Niño event (lag = −12 months), and then it reaches the western boundary about 15 months later (lag = −3 months), when the negative VAT anomaly at the equator begins to propagate eastward. Thus the VAT anomalies with westward propagation off the equator and eastward propagation at the equator play a negative feedback mechanism in the ENSO cycle simulated by the coupled model, which is very similar to the so–called delayed oscillator as proposed by Schopf and Suares (1988) and Battisti and Hirst (1989). But the physical mechanism associated with the ENSO cycle in the coupled mode may not be identical with that in the delayed oscillator, because meridional resolution of the model at the equator is too coarse to describe the Kelvin wave correctly that plays a crucial role in the delayed oscillator hypotheses.

As known well, the El Niño / Southern Oscillation (ENSO) is the strongest signal of interannual variation in the tropical Pacific, while a lot of analyses have suggested that the similar interannual variation but independent of ENSO signal has been found in the Indian Ocean (Saji et al., 1999, hereafter referred to as SGVY99; Webster et al., 1999; Anderson, 1999). SGVY99 defined the difference in SST anomaly between the tropical western Indian Ocean (50°–70°E, 10°S–10°N) and the tropical eastern Indian Ocean (90°–110°E, 10°S–0°) as a dipole model index (DMI), and found very close relationship between DMI and wind stress as well as precipitation in the tropical Indian Ocean. SGVY99 suggest that the dipole pattern may be attributed to the air–sea interaction in the tropical Indian Ocean.

In this study, the similar analyses are conducted as SGVY99 except for data from the coupled model. The regionally averaged SST anomalies in the tropical western and eastern Indian Ocean are shown in Figs. 10a and 10b, respectively, and the difference between them, referred to DMI, is shown in Fig. 10c. The significant correlation can be found among three time series, e.g., the correlations between DMI and SST anomalies in the western and eastern

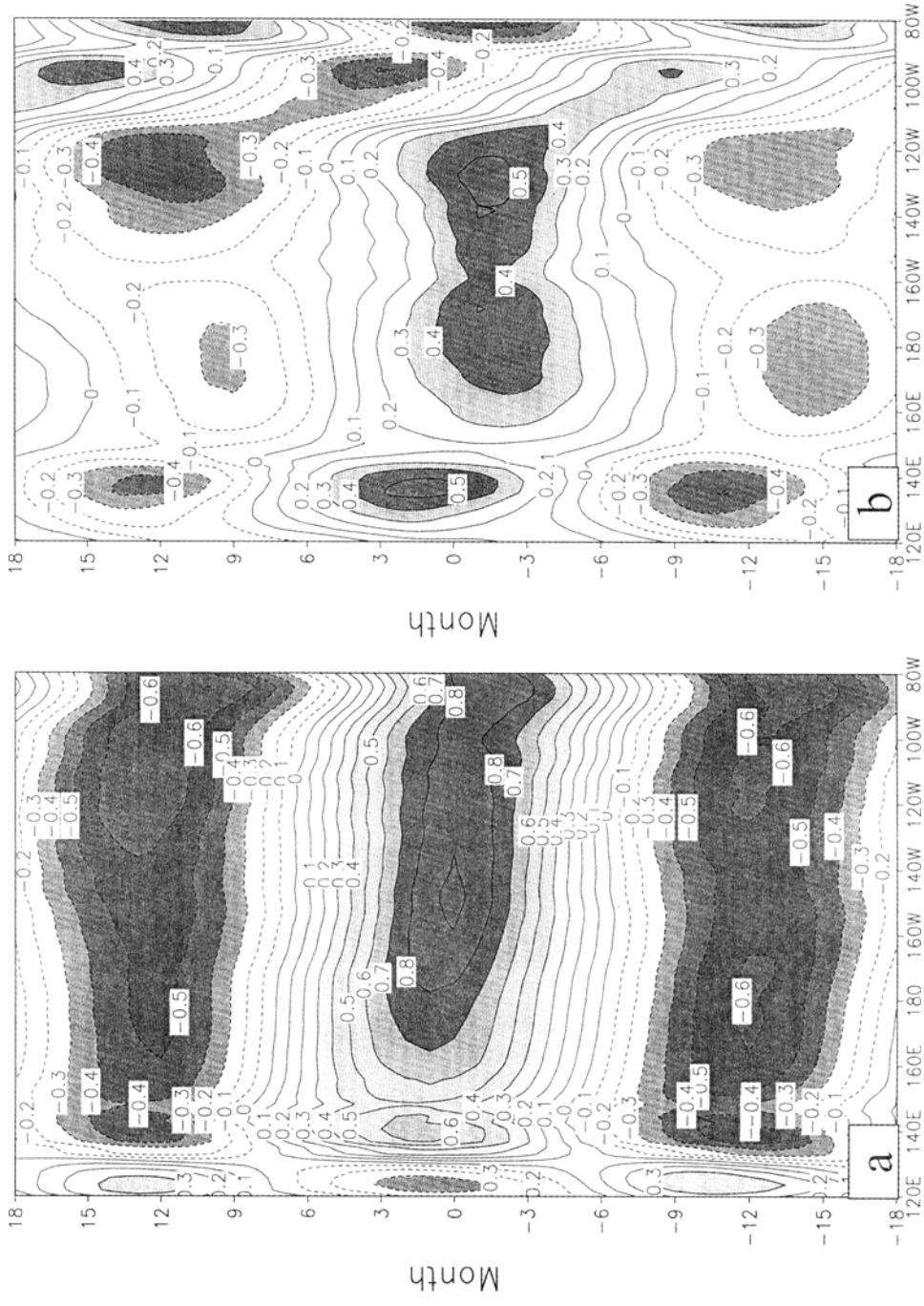
Month
18
15
12
9
6
3
0
-3
-6
-9
-12
-15
-18
120E
140E
160E
180
160W
140W
120W
100W
80W
a
b

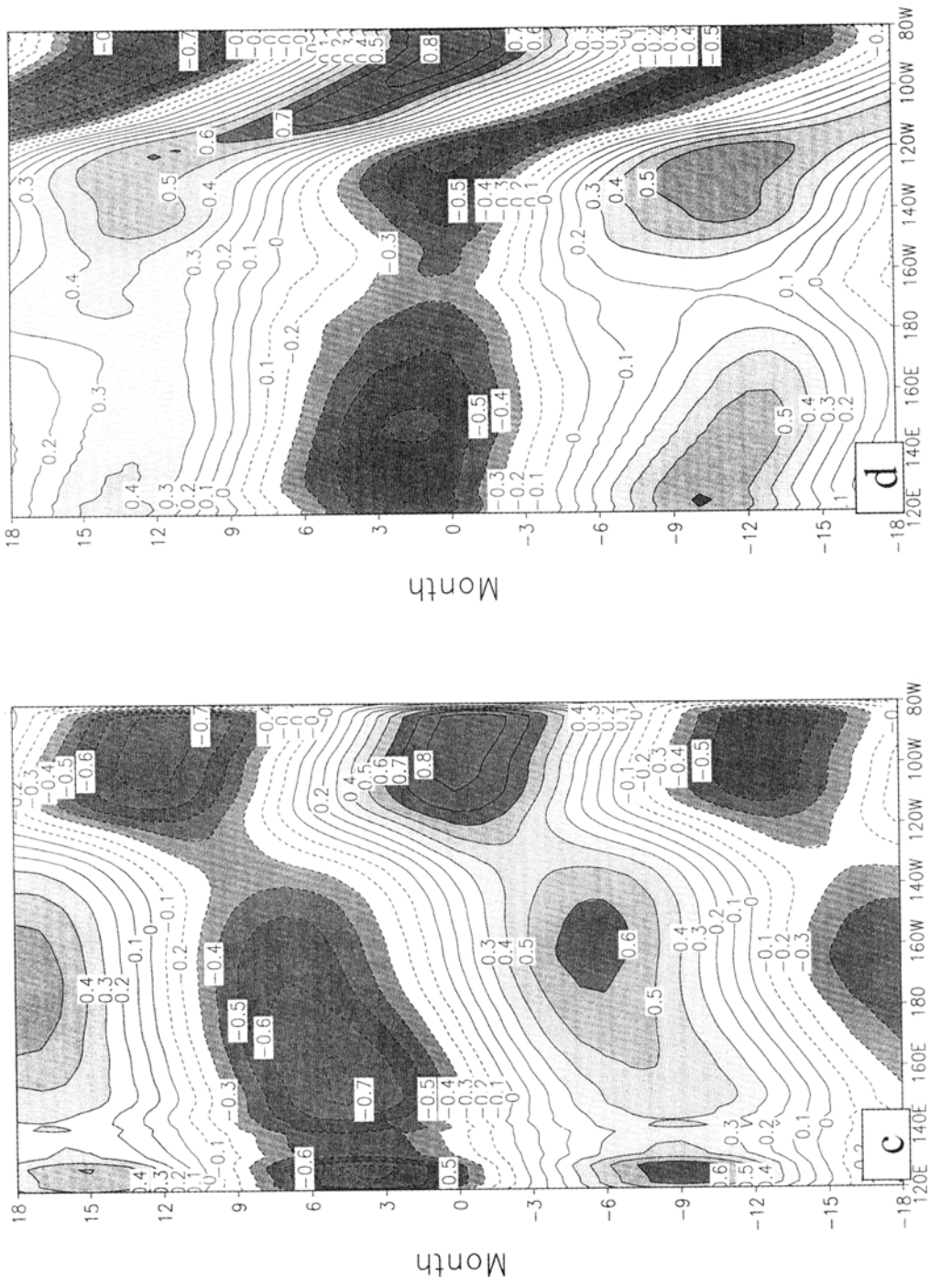

Fig. 9. Temporal evolution of lag correlation coefficients of Niño 3.4 SST index with (a) SST averaged from 5°S–5°N, (b) zonal wind stress, (c) vertically averaged temperatures (VAT) in the upper 300 m averaged from 5°S–5°N, (d) vertically averaged temperatures in the upper 300 m averaged from 5°–8°N.

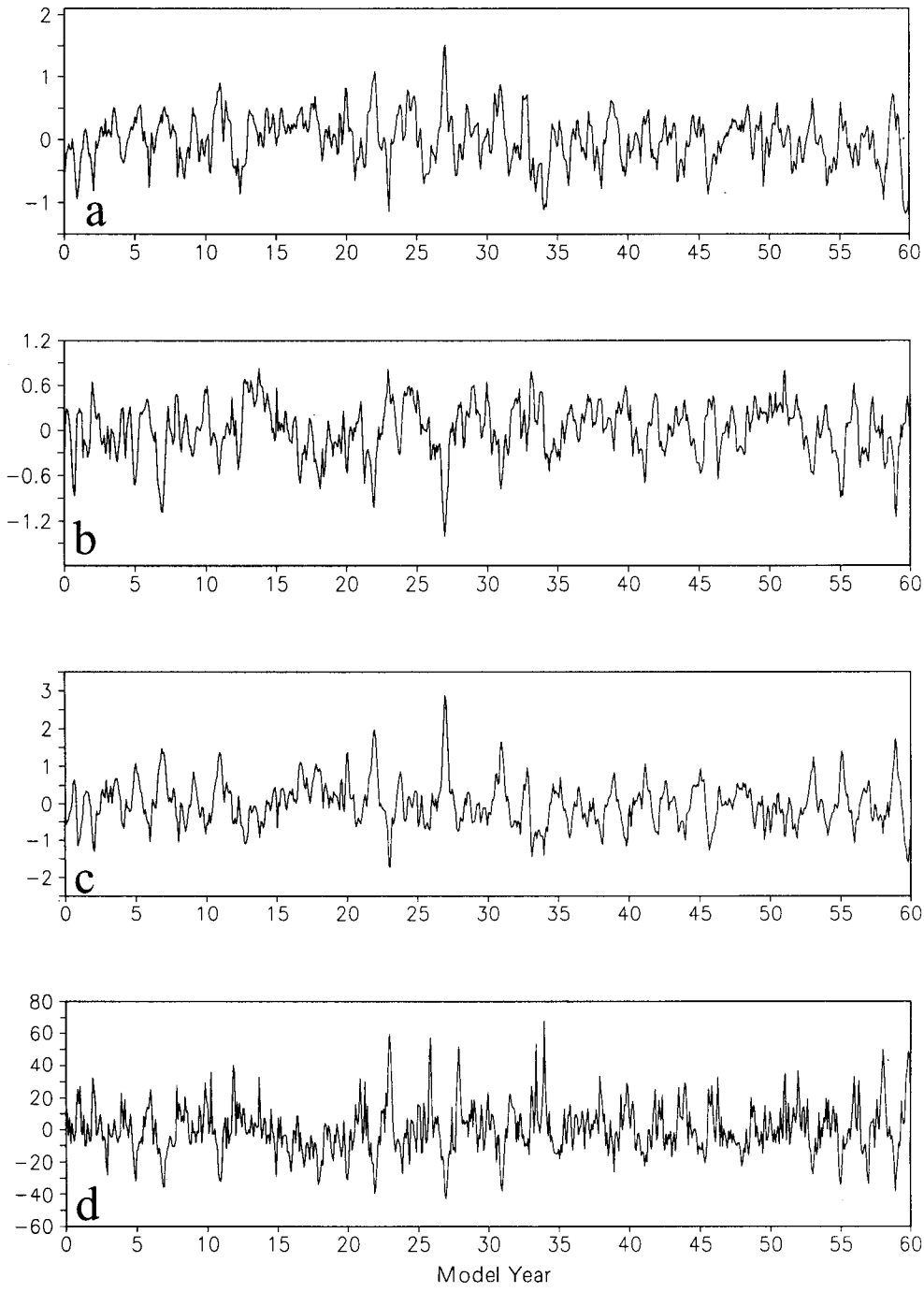

Fig. 10. Time series of sea surface temperature anomalies (°C) averaged from (a) 50°–70°E 10°S–10°N, and (b) 90°–110°E 10°S–0°, (c) the dipole mode index in the Indian Ocean (see section 4), (d) the zonal wind stress anomaly (10^{-3} N m^{-2}).

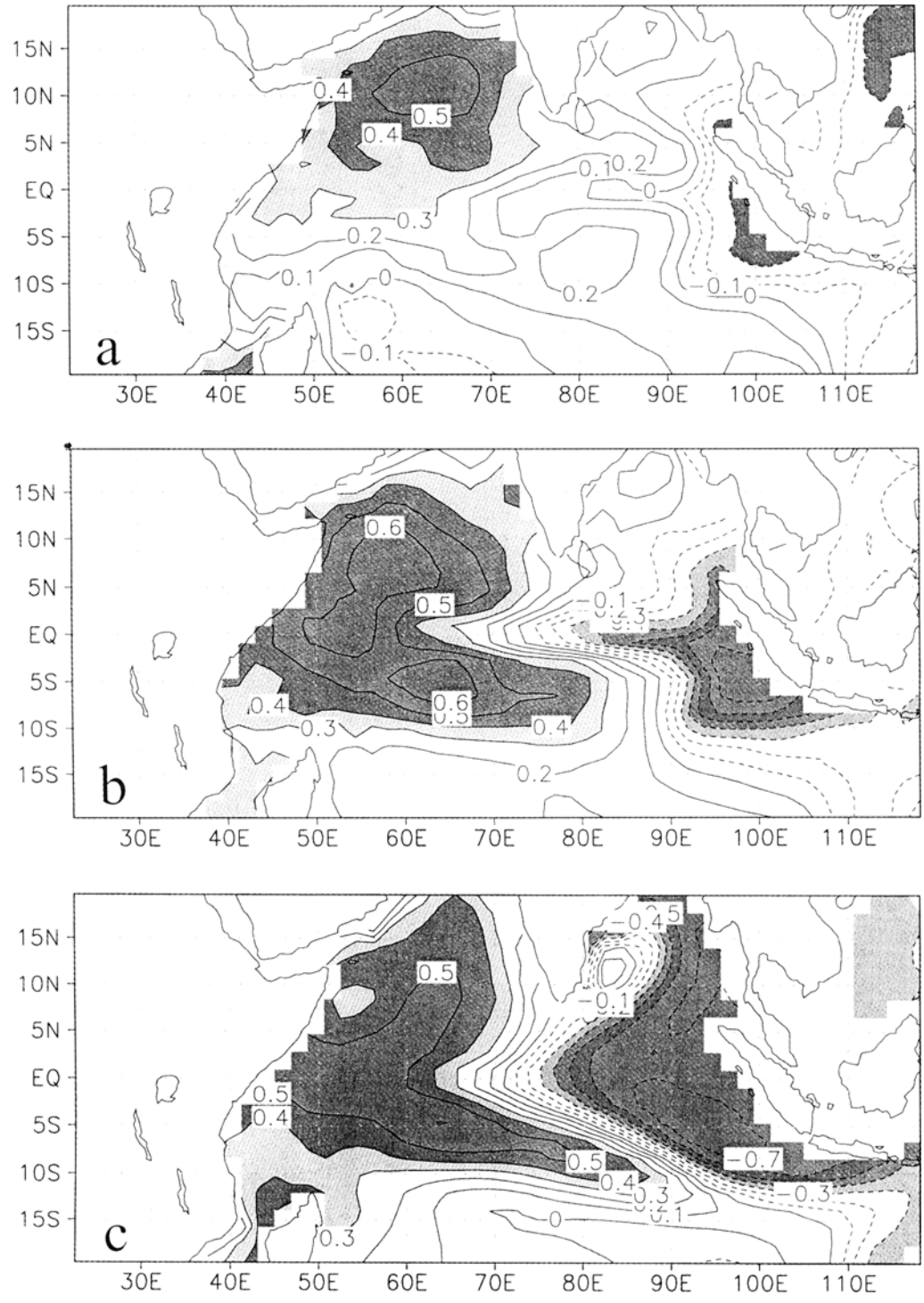
15N
10N
5N
EQ
5S
10S
15S
30E
40E
50E
60E
70E
80E
90E
100E
110E
a
0.4
0.5
0.4
0.1
0.2
0
0.3
0.2
0.1
0
0.2
−0.1
0
−0.1
b
0.6
0.5
−0.1
0.4
0.6
0.4
0.3
0.4
0.2
c
−0.5
0.5
−0.1
0.5
0.4
0.5
−0.7
0.4
0.3
−0.3
0.1
0
0.3

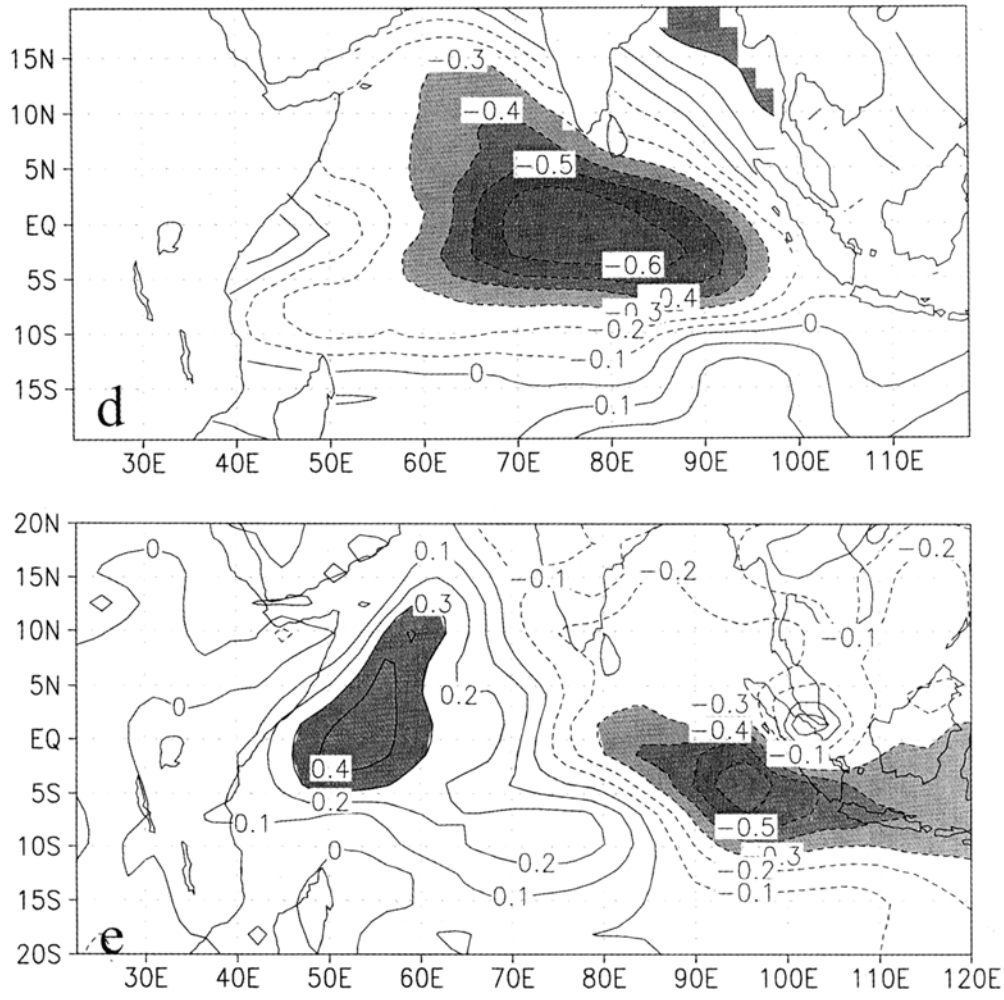

Fig. 11. Correlation coefficients of Niño 3.4 SST index with (a) SST, (b) correlation coefficients of dipole mode index with SST, (c) vertically averaged temperatures in the upper 300 m, (d) zonal wind stress and (e) precipitation in the Indian Ocean.

Indian Ocean are 0.83 and −0.78, respectively. The correlation coefficient between the DMI and the Niño 3.4 index is 0.44, which is not very strong but still significant. It implies that the simulated dipole mode in the tropical Indian Ocean is associated with the ENSO event in the coupled model. In addition, there is a strong correlation between the DMI and zonal wind stress averaged over the central and eastern Indian Ocean (70°–90°E, 5°S–5°N) (Fig. 10d), the correlation coefficient is −0.72, which is also similar to the observational one as described by SGVY99.

Here we calculate the correlation between the Niño 3.4 index and SST in the tropical Indian Ocean (Fig. 11a), and the DMI and SST (Fig. 11b), VAT (Fig. 11c), zonal wind stress (Fig. 11d) and precipitation (Fig. 11e). Although there is a significant positive correlation between Niño 3.4 index and SST in the northwestern Indian Ocean, the dipole mode pattern as

in Fig. 11b cannot be found. In fact, the dipole mode pattern exists not only in SST, but also in the subsurface with a clearer pattern (Fig. 11c). When the DMI is positive, e.g. the cold SST anomaly occurs in the eastern Indian Ocean and the warm SST anomaly in the western Indian Ocean, the zonal wind stress is enhanced (Fig. 11d). It implies that the zonal wind stress dominates the variation in SST and VAT; in other words, the dipole mode pattern should be attributed to the air–sea interaction in the Indian Ocean. As a result of the dipole pattern in SST, the precipitation also shows the similar pattern (Fig. 11e), it increases over the warm ocean and decreases over the cold ocean. The similar pattern has been found from the observational precipitation (See Fig. 4 in SGVY99).

5. Summary and discussion

The flexible coupled ocean–atmosphere general circulation model version 0 (FGCM–0) has been successfully integrated for 60 years. Some general characteristics of model climatology are examined to evaluate the ability of the coupled model in simulating the contemporary climate and its interannual variability in this study.

Although the flux correction is not employed in the coupled model FGCM–0, the model does not show the obvious climate drift. This is because that all component models, NCAR CCM3, land model, sea ice model, as well as IAP OGCM, show good ability to depict dynamical and physical processes in the climate system, in the meantime the flux coupler, which assures the conservation of energy and mass at the interfaces of model components, also plays an very important role in controlling the climate drift.

Compared to the observed climatology, the model's major errors are the simulated double ITCZ and the associated SST pattern. As described by a lot of studies (Mechoso et al., 1995; BG98), they are common features for the coupled models without flux correction. Analyses on heat budget in the coupled model indicate that the double ITCZ can be traced back to the overestimation of net solar radiation at the sea surface, which should be attributed to the error in the simulation of cloud in AGCM. In addition, there is about 10° southward extension of sea ice from the coupled model FGCM–0 than that from observation due to lower surface air temperature from the atmosphere–only model CCM3 over the Northwest Pacific Ocean.

Although the mean climatology from FGCM–0 is very similar to that from CSM–1, the FGCM–0 shows some different features of interannual variability. For the simulations of ENSO–like events, the FGCM–0 shows considerable regular oscillation around 2 years, but the CSM–1 shows a wider spectrum from 2 years to 7 years. The short oscillation period seems to be attributed to the faster phase speed of the eastward propagation of the heat content in the upper ocean in FGCM–0 than the observational one, e.g. the phase speed is about 0.6 m / s for FGCM–0, 0.3 m / s for CSM–1 and 0.2 m / s for observation. The main difference between the coupled model FGCM–0 and NCAR CSM–1 is the ocean component model, the IAP L30T63 is adopted for the former and the NCAR ocean model (NCOM) (Gent et al., 1998) is adopted for the latter. The NCOM configuration for NCAR CSM–1 has 2.4° in longitude and variable resolution in latitude, with minimum spacing 1.2° at the equator and in the Arctic Ocean and maximum spacing about 2.3° at middle latitudes. In the vertical, 45 levels are used, with 4 equal depth layers in the upper 50 m and 25 layers in the upper 1000 m in the ocean. The principal physical processes distinguishing L30T63 are the non–local K profile boundary layer parameterization (Large et al., 1994) and the third–order upstream differencing used for heat and salt (Holland et al., 1998). Although there are a lot of differ-

ences between L30T63 and NCOM, but the coarse meridional resolution at the equator may be responsible for too fast eastward propagation of VAT in the coupled model FGCM–0, because the high meridional resolution is crucial for the model to describe the Kelvin wave correctly.

In the tropical Indian Ocean, the coupled model FGCM–0 shows a similar dipole mode pattern to the observational one. The simulated dipole mode pattern is not only shown in SST, but also in VAT, especially there is close correlation between dipole mode index and the zonal wind stress in the central Indian Ocean, which implies that the dipole mode pattern is a coupled mode resulting from the air–sea interaction in the tropical Indian Ocean. In the meanwhile, not as shown in SGVY99, the simulated DMI is closely related to the Niño 3.4 index in the coupled model. In fact, the relationship between ENSO and the dipole mode may be very complex, for example, Yu and Rienecker (2000) indicated that the strong El Niño events favor the dipole mode events in the Indian Ocean, i.e. the dipole events coincide with El Niño events in some years such as 1972 and 1997. Because the coupled model can reproduce El Niño and dipole events simultaneously, it may be a beneficial tool to study the physical link between them in the future.

The authors wish to thank Prof. Wang Bin for the helpful discussion in the simulation of the Indian Ocean dipole pattern. The extended integration of FGCM–0 would not have been finished without the help from the computer center of China Academy of Meteorological Sciences. We wish to thank Mr. Meng Nianqing for helping us tune the paralleling FGCM–0 codes.

REFERENCES

Anderson, D., 1999: Extremes in the Indian Ocean. *Nature*, **401**, 337–338.

Battisti, D. S., and A. C. Hirst, 1989: Interannual variability in a tropical atmosphere–ocean model: Influence of the basic state, ocean geometry and nonlinearity. *J. Atmos. Sci.*, **46**, 1687–1712.

Bonan, G. B., 1998: The land surface climatology of the NCAR land surface model coupled to the NCAR community climate model. *J. Climate*, **11**, 1307–1326.

Boville, B. A., and P. R. Gent, 1998: The NCAR climate system model, Version One. *J. Climate*, **11**, 1115–1130.

Boville, B. A., and J. W. Hurrell, 1998: A comparison of the atmospheric circulations simulated by the CCM3 and CSM1. *J. Climate*, **11**, 1327–1341.

Chen Keming, Zhang Xuehong, Jin Xiangze, and Lin Wuyin, 1997: A global coupled ocean–atmosphere model for studying global climate change, I: Model configuration and performance. *Acta Oceanologica Sinica*, **19(3)**, 22–32 (in Chinese).

Covey, C., 1994: Global ocean circulation and equator–pole heat transport as a function of ocean GCM resolution, Report No.19, Program for Climate Model Diagnosis and Intercomparison (Lawrence Livermore National Laboratory, Livermore, CA), 30pp.

da Silva, A. M., C. C. Young, and S. Levitus, 1994: Atlas of surface marine data 1994, Vol.1: Algorithms and procedures, NOAA Atlas NECDIS 6, U.S. Dept. of Commerce, Washington, DC, 83pp.

Gates, W. L., 1992: AMIP: The atmospheric model intercomparison project. *Bull. Amer. Meteor. Soc.*, **72**, 1962–1970.

Gent, P. R., and J. C. McWilliams, 1990: Isopycnal mixing in ocean circulation models. *J. Phys. Oceanogr.*, **20**, 150–155.

Gent, P. R., F. O. Bryan, G. Danabasoglu, S. C. Doney, W. R. Holland, W. G. Large, and J. C. McWilliams, 1998: The NCAR climate system model global ocean component. *J. Climate*, **11**, 1287–1306.

Gloersen, P., W. J. Campbell, D. J. Cavalieri, J. C. Comiso, C. L. Parkinson, and H. J. Zwally, 1992: Arctic and Antarctic Sea Ice, 1978–1987: Satellite passive–microwave observations and analysis. U.S. Natl. Aeron. Space Admin. Special Publ. NASA SP–511, 290pp.

Haney, R. L., 1971: Surface thermal boundary condition for ocean circulation models. *J. Phys. Oceanogr.*, **1**, 241–248.

Hellerman, S., and Rosenstein, M., 1983: Normal monthly wind stress data over the world ocean with error estimates. *J. Phys. Oceanogr.*, **13**, 1093–1104.

Holland, W. R., J. H. C. Chow, and F. O. Bryan, 1998: Application of a third-order upwind scheme in the NCAR ocean model. *J. Climate*, **11**, 1487–1493.

Jin Xiangze, Zhang Xuehong, and Zhou Tianjun, 1999: Fundamental framework and experiments of the third generation of IAP / LASG world ocean general circulation model. *Advances in Atmospheric Sciences*, **16(2)**, 197–215.

Kiehl, J. F., J. J. Hack, G. B. Bonan, B. A. Boville, D. L. Williamson, and P. J. Pasch, 1998: The National Center for Atmospheric Research community climate model: CCM3. *J. Climate*, **11**, 1131–1149.

Large, W. G., J. C. McWilliams, and S. C. Doney, 1994: Ocean mixing: A review and a model with a nonlocal boundary layer parameterization. *Rev. Geophys.*, **32**, 363–403.

Levitus, S., and T. P., Boyer, 1994: World Ocean Atlas 1994 Volume 3:Salinity, NOAA Atlas NESDIS3. U. S. Department of Commerce, Washington, D. C. 99pp.

Mechoso, C. R., and Coauthors, 1995: The seasonal cycle over the tropical Pacific in coupled ocean–atmosphere general circulation models. *Mon. Wea. Rev.*, **123**, 2825–2838.

Meehl, A. M., 1995, Global coupled general circulation models. *Bull. Amer. Meteor. Soc.*, **76**, 951–957.

Meehl, A. M., and J. M. Arblaster, 1998: The Asian–Australian monsoon and El Niño–Southern Oscillation in the NCAR climate system model. *J. Climate*, **11**, 1356–1385.

Meehl, G. A., G. J. Boer, C. Covey, M. Latif, and R. J. Stouffer, 2000: The coupled model intercomparison project (CMIP). *Bull. Amer. Meteor. Soc.*, **81**, 313–318.

Pacanowski, R. C, and G. Philander, 1981: Parameterization of vertical mixing in numerical models of the tropical ocean. *J. Phys. Oceanogr.*, **11**, 1442–1451.

Parkinson, C. L., and W. M. Washington, 1979: A large-scale numerical model of sea ice. *J. Geophys. Res.*, **84**, 311–337.

Philander, S. G. H., D. Gu, D. Halpern, G. Lambert, N. -C. Lau, T. Li, and R. C. Pacanowski, 1996: Why the ITCZ is mostly north of the equator. *J. Climate*, **9**, 2958–2972.

Rosati, A, and K., Miyakoda, 1988: A general circulation model for upper ocean circulation. *J. Phys. Oceanogr.*, **18**, 1601–1626.

Saji, N. N., B. N. Goswami, P. N. Vinayachandran, and T. Yamagata, 1999: A dipole mode in the tropical Indian Ocean. *Nature*, **401**, 360–363.

Shea, D. J., K. E. Trenberth, and R. W. Reynolds, 1990: A global monthly mean sea surface temperature climatology. NCAR Tech. Note NCAR / TN–345, 167pp.

Schopf, P. S., and M. J. Suares, 1988: Vacillations in a coupled ocean–atmosphere model. *J. Atmos. Sci.*, **45**, 549–566.

Weatherly, J. W., B. P. Briegleb, W. G. Large, and J. A. Maslanik, 1998: Sea ice and polar climate in the NCAR CSM. *J. Climate*, **11**, 1472–1486.

Webster, P. J., A. Moore, J. Loschnigg, and R. Leben, 1999: Coupled ocean–atmosphere dynamics in the Indian Ocean. *Nature*, **401**, 356–360.

Wu Guoxiong, and Coauthors, 1997: Global ocean–atmosphere–land system model of LASG (GOALS / LASG) and its performance in simulation study. *Quart. J. Appl. Meteor.*, **8** (Supplement Issue), 15–28 (in Chinese).

Ye Zhengqing, Dong Min, and Chen Jiabin, 2000: Simulated climate by National Climate Center GCM with the observed SST Study on the Short-range Climate Prediction System of China, Ding et al., Eds., China Meteorological Press, Beijing, 70–78pp. (in Chinese).

Yu Lisan, and M. M. Rienecker, 2000: Indian Ocean warming of 1997–1998. *J. Geophys. Res.*, **105**, 16923–16939.

Yu Yongqiang, A. Izard, Zhang Xuehong, and Guo Yufu, 2001: The response of IAP / LASG OGCM to wind stress. *Chinese J. Atmos. Sci.*, **25**, 721–739 (in Chinese).

Yu Yongqiang, Zhang Xuehong, Liu Hui, and Jin Xiangze, 2000: Schemes for coupling AGCM and OGCM. *IAP Global Ocean–Atmosphere–Land System Model*, Zhang et al., Eds., Science Press, Beijing, 100–114pp.

Zhang Xuehong, Bao Ning, Yu Rucong, and Wang Wanqiu, 1992: Coupling scheme experiments based on an atmospheric and an oceanic GCM. *Chinese Journal of Atmospheric Sciences*, **16**, 129–144.

一个灵活的海洋–大气耦合环流模式

俞永强　宇如聪　张学洪　刘海龙

摘　要

在美国国家大气研究中心(NCAR)气候系统模式(CSM–1)的基础上，通过使用中国科学院大气物理研究所发展的 T63／L30 全球海洋环流模式替代 CSM–1 的海洋分量模式以及其它一些必要的改动发展了一个灵活的海气耦合环流模式的初始版本(FGCM–0)。在耦合模式 FGCM–0 的几十年的 spun–up 试验之后，这个耦合模式在没有使用任何通量订正的情形下积分了 60 年。该模式不仅显示了合理的长期平均气候，而且可以重现许多年际气候变化的特征，如类似 ENSO 的事件和赤道印度洋的偶极子模态。与 NCAR 的 CSM–1 相比，可以发现一些共同存在的问题，如对北太平洋海冰的过高估计和模拟的双"赤道辐合带(ITCZ)"现象等。进一步的分析表明，这些现象可能是由大气模式本身的误差引起的。

关键词: 耦合模式，ENSO，气候漂移